Improvement in the Thermoelectric Figure of Merit by La/Ag Cosubstitution in PbTe

Kyunghan Ahn,[†] Changpeng Li,[‡] Ctirad Uher,[‡] and Mercouri G. Kanatzidis*,[†]

Department of Chemistry, Northwestern University, Evanston, Illinois 60208, and Department of Physics, University of Michigan, Ann Arbor, Michigan 48109

Received December 19, 2008. Revised Manuscript Received January 27, 2009

The thermoelectric properties of La-doped and Ag/La codoped PbTe were investigated in the temperature range of 300 to ~720 K. All samples crystallize in the NaCl-type structure without noticeable secondary phase and exhibit narrow bandgaps of 0.26−0.30 eV, typical of PbTe. La doping (≤5 at %) in PbTe significantly enhances the room temperature electrical conductivity to >5000 S/cm, indicating that La is an efficient electron donor. Hall coefficient data confirm the significant increase in electron carrier concentration from $\sim 2 \times 10^{18}$ cm^{-3} at 300 K for PbTe to $\sim 5.3 \times 10^{19}$ cm^{-3} for $Pb_{0.99}La_{0.01}Te$, and $\sim 1.7 \times 10^{20}$ cm^{-3} for $Pb_{0.95}La_{0.05}Te$. Ag doping in $Pb_{0.99}La_{0.01}Te$ has an opposite effect on the electron carrier concentration ($\sim 2.0 \times 10^{19}$ cm^{-3} at 300 K for $Ag_{0.05}Pb_{0.99}La_{0.01}Te$ and $\sim 1.5 \times 10^{19}$ cm^{-3} for $Ag_{0.1}Pb_{0.99}La_{0.01}Te$), consistent with the role of Ag as electron acceptor. The temperature dependence of mobility is discussed in detail using the physics of electron scattering and possible scattering mechanisms. For $Ag_{0.05}Pb_{0.99}La_{0.01}Te$, a high power factor of ~22 μW/(cm K^2) at ~720 K was achieved with the optimal total thermal conductivity of ~ 1.3 W/(m K) at ~720 K, giving a maximum figure of merit $ZT \approx 1.2$ at ~720 K.

Introduction

Currently, there is growing interest in the field of thermoelectrics (TE) for power generation driven by both the need for higher performance TE materials and the recent progress in enhancing the figure of merit.[1−5] The thermoelectric figure of merit is defined $ZT = S^2\sigma T/\kappa$, where S, σ, T, and κ are the thermopower (Seebeck coefficient), electrical conductivity, absolute temperature, and thermal conductivity, respectively. High-efficiency thermoelectric materials require a large Seebeck coefficient, high electrical conductivity, and low thermal conductivity. Enhancing ZT is challenging because of the interdependence of physical parameters that define it. Significant progress in raising ZT has been recently accomplished, namely for filled skutterudite antimonides,[6,7] $AgPb_mSbTe_{2+m}$ (LAST-m),[8] $NaPb_mSbTe_{2+m}$ (SALT-m),[9] $Ag_x(Pb,Sn)_mSb_yTe_{2+m}$ (LASTT-m),[10] PbTe-PbS,[11] PbTe:Tl,[12] and PbTe−Pb-Sb,[13] and thin-film multilayers.[14,15]

Lanthanide elements in PbTe are expected to be effective donors because of their trivalent character. To the best of our knowledge, the thermoelectric properties of bulk $Pb_{1-x}RE_xTe$ systems (RE = rare earth elements) have not been extensively studied.[16−20] In this paper, we investigated the substitution of La for Pb, $Pb_{1-x}La_xTe$ ($x = 0$, 0.01, 0.03, 0.05), and the effect of Ag as a p-type codopant on the sample of $Pb_{0.99}La_{0.01}Te$. Namely, we studied the compositions $Ag_yPb_{0.99}La_{0.01}Te$ ($y = 0$, 0.01, 0.03, 0.05, 0.1, 0.15). Hall coefficient measurements verified that La is a good electron donor, whereas Ag acts as an electron acceptor. We discuss the temperature dependences of mobility through the

* Corresponding author. E-mail: m-kanatzidis@northwestern.edu.
[†] Northwestern University.
[‡] University of Michigan.

(1) Wood, C. *Rep. Prog. Phys.* **1988**, *51*, 459.
(2) (a) Mahan, G.; Sales, B.; Sharp, J. *Phys. Today* **1997**, *50*, 42. (b) Chung, D. Y.; Iordanidis, L.; Choi, K. S.; Kanatzidis, M. G. *Bull. Kor. Chem. Soc.* **1998**, *19*, 1283–1293.
(3) DiSalvo, F. J. *Science* **1999**, *285*, 703.
(4) Dresselhaus, M. S.; Chen, G.; Tang, M. Y.; Yang, R.; Lee, H.; Wang, D.; Ren, Z.; Fleurial, J.-P.; Gogna, P. *Adv. Mater.* **2007**, *19*, 1043.
(5) Snyder, G. J.; Toberer, E. S. *Nat. Mater.* **2008**, *7*, 105.
(6) Sales, B. C.; Mandrus, D.; Williams, R. K. *Science* **1996**, *272*, 1325.
(7) Uher, C. In *Thermoelectrics Handbook, Macro to Nano*; Rowe, D. M., Ed.; CRC Press: Boca Raton, FL, 2006; Chapter 34.
(8) Hsu, K. F.; Loo, S.; Guo, F.; Chen, W.; Dyck, J. S.; Uher, C.; Hogan, T.; Polychroniadis, E. K.; Kanatzidis, M. G. *Science* **2004**, *303*, 818.
(9) (a) Poudeu, P. F. P.; D'Angelo, J.; Downey, A. D.; Short, J. L.; Hogan, T. P.; Kanatzidis, M. G. *Angew. Chem., Int. Ed.* **2006**, *45*, 3835. (b) Quarez, E.; Hsu, K. F.; Pcionek, R.; Frangis, N.; Polychroniadis, E. K.; Kanatzidis, M. G. *J. Am. Chem. Soc.* **2005**, *127*, 9177–9190.
(10) (a) Androulakis, J.; Hsu, K. F.; Pcionek, R.; Kong, H.; Uher, C.; D'Angelo, J. J.; Downey, A.; Hogan, T.; Kanatzidis, M. G. *Adv. Mater.* **2006**, *18*, 1170. (b) Poudeu, P. F. P.; D'Angelo, J.; Kong, H. J.; Downey, A.; Short, J. L.; Pcionek, R.; Hogan, T. P.; Uher, C.; Kanatzidis, M. G. *J. Am. Chem. Soc.* **2006**, *128*, 14347–14355.
(11) Androulakis, J.; Lin, C.-H.; Kong, H.-J.; Uher, C.; Wu, C.-I.; Hogan, T.; Cook, B. A.; Caillat, T.; Paraskevopoulos, K. M.; Kanatzidis, M. G. *J. Am. Chem. Soc.* **2007**, *129*, 9780.
(12) Heremans, J. P.; Jovovic, V.; Toberer, E. S.; Saramat, A.; Kurosaki, K.; Charoenphakdee, A.; Yamanaka, S.; Snyder, G. J. *Science* **2008**, *321*, 554.
(13) Sootsman, J. R.; Kong, H.; Uher, C.; D'Angelo, J. J.; Wu, C.-I.; Hogan, T. P.; Caillat, T.; Kanatzidis, M. G. *Angew. Chem., Int. Ed* **2008**, *47*, 8618.
(14) Harman, T. C.; Taylor, P. J.; Walsh, M. P.; LaForge, B. E. *Science* **2002**, *297*, 2229.
(15) Venkatasubramanian, R.; Siivola, E.; Colpitts, T.; O'Quinn, B. *Nature* **2001**, *413*, 597.
(16) Iskender Zade, Z. A.; Abilov, C. I.; Faradzhev, V. D.; Zeinalov, E. Z.; Kurbanov, E. M. *Inorg. Mater.* **1990**, *26*, 366.
(17) Alekseeva, G. T.; Vedernikov, M. V.; Gurieva, E. A.; Konstantinov, P. P.; Prokofeva, L. V.; Ravich, Yu. I. *Semiconductors* **1998**, *32*, 716.
(18) Nouneh, K.; Kityk, I. V.; Viennois, R.; Benet, S.; Charar, S.; Paschen, S.; Ozga, K. *Phys. Rev. B* **2006**, *73*, 035329.
(19) Nouneh, K.; Plucinski, K. J.; Bakasse, M.; Kityk, I. V. *J. Mater. Sci.* **2007**, *42*, 6847.
(20) Ozga, K.; Nouneh, K.; Slezak, A.; Kityk, I. V. *J. Alloys Compd.* **2008**, *448*, 49.

10.1021/cm803437x CCC: $40.75
Published on Web 03/19/2009

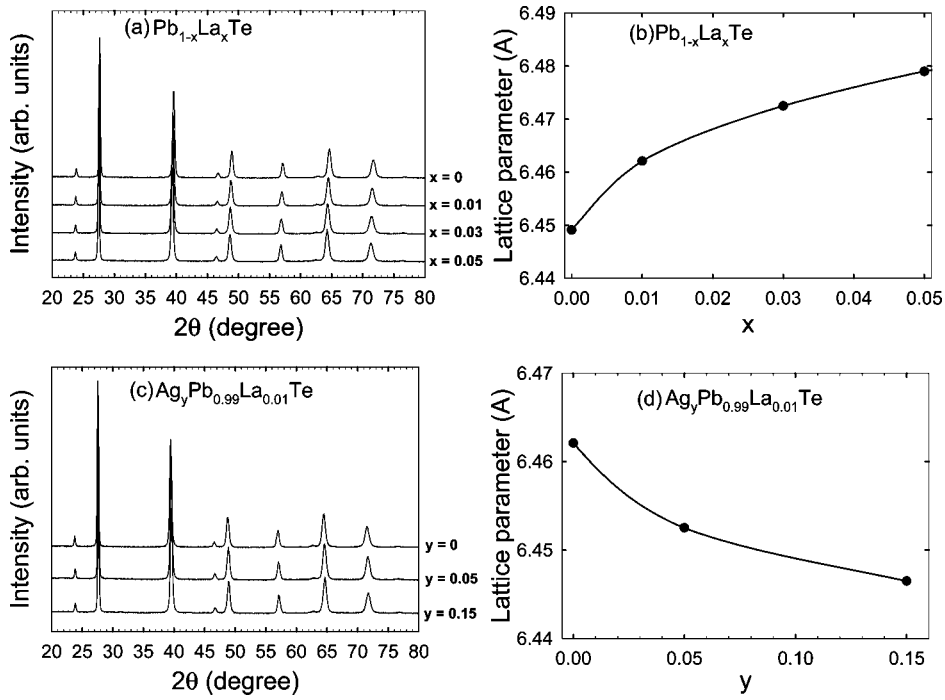

Figure 1. (a) Powder X-ray diffraction patterns of samples of $Pb_{1-x}La_xTe$ ($0 \le x \le 0.05$), (b) variation in the lattice parameters as a function of x for $Pb_{1-x}La_xTe$, (c) powder X-ray diffraction patterns of samples of $Ag_yPb_{0.99}La_{0.01}Te$ ($0 \le y \le 0.15$), and (d) variation in the lattice parameters as a function of y for $Ag_yPb_{0.99}La_{0.01}Te$. The lattice parameters were refined by using a full profile Rietveld refinement technique.[35]

underlying physics of electron scattering and the possible scattering mechanism. The incorporation of Ag was critical to obtain a high power factor and an optimized $ZT \approx 1.2$ at ~720 K for $Ag_{0.05}Pb_{0.99}La_{0.01}Te$.

Experimental Section

Synthesis. Ingots with nominal compositions of $Pb_{1-x}La_xTe$ ($x = 0$, 0.01, 0.03, and 0.05) and $Ag_yPb_{0.99}La_{0.01}Te$ ($y = 0$, 0.01, 0.03, 0.05, 0.1, and 0.15) were prepared by heating the mixture of high purity starting elemental materials of Ag (coin, 99.99%), Pb (Rotometals, 99.99%), La (Cerac Inc., 40 mesh, 99.9%), and Te (Atlantic Metals, 99.999%) in carbon-coated fused silica tubes under a vacuum (the residual pressure of $\sim 1 \times 10^{-4}$ Torr) at ~1323 K for 10 h (including 2 h rocking to facilitate complete mixing and homogeneity of the liquid phase) and cooling to ~973 K in 48 h finally followed by cooling to room temperature over 12 h. Single dense ingots were obtained with a dark silvery metallic shine. The ingots are stable in water and air and are relatively strong.

Powder X-ray Diffraction and Infrared Spectroscopy. Fine powder samples of $Pb_{1-x}La_xTe$ and $Ag_yPb_{0.99}La_{0.01}Te$ were examined by X-ray diffraction using Cu Kα radiation and room temperature optical diffuse reflectance measurements as described previously.[21]

Thermal Conductivity. The thermal diffusivity (D) was directly measured under nitrogen atmosphere and the specific heat (C_p) was indirectly derived using a standard sample (pyroceram) as a function of temperature from room temperature to ~720 K using the flash diffusivity method in a NETZSCH LFA 457 MicroFlash instrument. In the flash diffusivity method, the front face of a disk shaped sample (~8 mm diameter and 1−2 mm thickness) is irradiated by a short laser burst, and the resulting rear face temperature rise is recorded and analyzed by an IR detector. The thermal conductivity (κ) was calculated from the equation $\kappa = DC_p\rho$, where ρ is the density of the sample, measured using sample dimensions and mass.

Electrical Properties. The samples were cut into rectangular shapes of ~3 mm × 3 mm × 9 mm for electrical property measurements. The longer direction coincides with the direction in which the thermal conductivity was measured. Electrical conductivity and thermopower were measured simultaneously under a helium atmosphere (~0.1 atm) from room temperature to ~720 K using a ULVAC-RIKO-ZEM3 measurement system.

Hall Measurements. The Hall coefficient was measured with a homemade high temperature apparatus, which provides a working range from 300 K to ~873 K. The sample was press mounted and protected with argon gas to avoid possible oxidization at high temperature. The Hall resistance was monitored with Linear Research AC Resistance Bridge (LR-700), with constant magnetic fields of ±1 T applied by using an Oxford Superconducting Magnet.

Results and Discussion

Powder X-ray Diffraction. Powder X-ray diffraction (PXRD) patterns and lattice parameters as a function of x for the $Pb_{1-x}La_xTe$ ($x = 0$, 0.01, 0.03, 0.05) samples are shown in panels a and b in Figure 1, respectively. The PXRD patterns (Figure 1a) indicate a single phase crystallizing in a cubic NaCl-type structure with the space group of $Fm\bar{3}m$. As expected, the lattice parameters (Figure 1b) expand with increasing La content because smaller Pb atoms (metallic radius ≈ 1.75 Å) are replaced by larger La atoms (metallic radius ≈ 1.88 Å).[22] The lattice parameters reach a finite value and then stop increasing with further increases of La content.

(21) Han, M.-K.; Hoang, K.; Kong, H.; Pcionek, R.; Uher, C.; Paraskevopoulos, K. M.; Mahanti, S. D.; Kanatzidis, M. G. *Chem. Mater.* **2008**, *20*, 3512.

(22) Teatum, E. T. Gschneidner, Jr., K. A. and Waber, J. T. *Compilation of Calculated Data Useful in Predicting Metallurgical Behavior of the Elements in Binary Alloy Systems*; Los Alamos National Laboratory Report No. LA-4003;, Los Alamos National Laboratory: Los Alamos, NM, 1968.

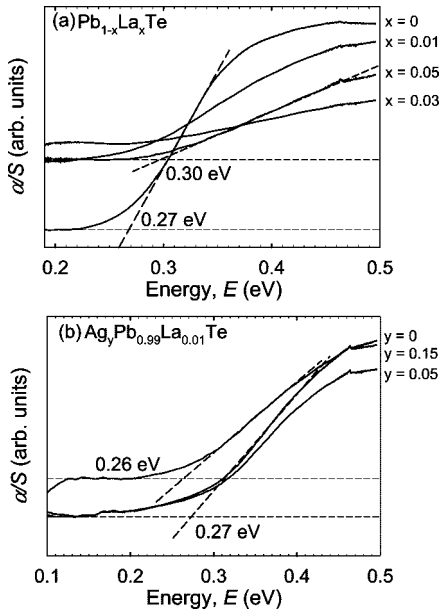

Figure 2. (a) Infrared absorption spectra and energy band gaps of samples of $Pb_{1-x}La_xTe$ ($0 \le x \le 0.05$) and (b) $Ag_yPb_{0.99}La_{0.01}Te$ ($0 \le y \le 0.15$).

This indicates a solubility limit of La in PbTe at ~3 at %, in agreement with a previous study.[16] The PXRD patterns of $Ag_yPb_{0.99}La_{0.01}Te$ ($y = 0$, 0.05, 0.15) in Figure 1c also shows a nearly single phase with a NaCl-type structure and the lattice parameters decrease with increasing Ag content (Figure 1d), indicating the substitution of larger Pb atoms with smaller Ag atoms (metallic radius ≈ 1.45 Å).

Typical infrared absorption spectra for the $Pb_{1-x}La_xTe$ ($x = 0$, 0.01, 0.03, 0.05) and $Ag_yPb_{0.99}La_{0.01}Te$ ($y = 0$, 0.05, 0.15) samples are shown in panels a and b in Figure 2, respectively. All samples exhibit spectroscopically observable energy bandgaps between 0.26 and 0.30 eV that are similar to those of pristine PbTe.

Charge Transport Properties. Panels a and b in Figure 3 show the temperature dependence of the electrical conductivity σ of $Pb_{1-x}La_xTe$ ($x = 0$, 0.01, 0.03, 0.05) and $Ag_yPb_{0.99}La_{0.01}Te$ ($y = 0$, 0.01, 0.03, 0.05, 0.10, 0.15) samples, respectively. For all samples, σ decreases with increasing temperature, indicating degenerate conduction for the entire measuring temperature range. For $Pb_{1-x}La_xTe$ (Figure 3a), all samples with $x = 0.01$, 0.03, and 0.05 show room temperature electrical conductivities above 5000 S/cm. By comparison pure PbTe sample with $x = 0$ prepared in this work showed room temperature electrical conductivity of ~400 S/cm. Thus, the La acts as an effective electron donor, consistent with the Hall coefficient data presented in this paper. The electrical conductivity of the $Ag_yPb_{0.99}La_{0.01}Te$ samples decreases with increasing y (Ag content); the room temperature σ values are of ~5600, ~4800, ~2900, ~3200, ~2300, and ~2000 S/cm for $y = 0$, 0.01, 0.03, 0.05, 0.1, and 0.15, respectively. The Ag in $Pb_{1-x}La_xTe$ plays a role as a good electron acceptor in reducing electron carriers, as confirmed by the Hall coefficient data.

The electrical conductivity of doped PbTe samples follows a temperature dependent power law of $\sigma \approx T^{-\delta}$ ($\delta \approx 2-3$). This reflects mainly the dependence of the mobility $\mu \approx T^{-n}$ ($n \approx 2-3$) as the extrinsic carrier concentration over the entire temperature range is approximately constant.[23] In this work, the value of δ decreases with increasing La content for $Pb_{1-x}La_xTe$ at 300−530 K (~2.6, ~1.6, ~1.0, and ~1.1 for $x = 0$, 0.01, 0.03, and 0.05, respectively). For the $Ag_yPb_{0.99}La_{0.01}Te$ samples, regardless of y, δ is 1.6−1.8 at 300−500 K. This is a different power law because δ is generally 2−3 for PbTe samples and is related with the mobility because, as we will show below, the carrier concentration is approximately invariant in the temperature range of 300−530 K.

The temperature-dependent thermopower data of $Pb_{1-x}La_xTe$ ($x = 0$, 0.01, 0.03, 0.05) and $Ag_yPb_{0.99}La_{0.01}Te$ ($y = 0$, 0.01, 0.03, 0.05, 0.10, 0.15) samples are shown in panels c and d in Figure 3, respectively. Negative values of thermopower over the entire temperature range indicate *n*-type conduction with the dominant charge carriers being electrons. It is therefore evident that donor La atoms sit on Pb sites in the crystal structure. The absolute value of thermopower for $Pb_{1-x}La_xTe$ ($x = 0.01$, 0.03, 0.05) and $Ag_yPb_{0.99}La_{0.01}Te$ ($y = 0$, 0.01, 0.03, 0.05, 0.10, 0.15) samples increases almost linearly with increasing temperature. The samples with $x = 0.03$ and 0.05 show thermopower values ranging from approximately −20 μV/K at ~300 K to approximately −80 μV/K at ~670 K, whereas for $x = 0.01$, the values range from around −60 μV/K at ~300 K to around −130 μV/K at ~670 K (Figure 3c). The absolute thermopower values of La-substituted samples are relatively small compared to pure PbTe (−290 μV/K at ~300 K and −320 μV/K at ~670 K), which indicates that La atoms contribute significantly to increasing the concentration of electron carriers in the sample. For the $Ag_yPb_{0.99}La_{0.01}Te$ samples, the thermopower of $y = 0.01$ is very small and similar to that of $y = 0$ over the entire temperature range. With increasing Ag content $y > 0.01$, the thermopower at ~300 K increases to between −80 and −100 μV/K and at ~670 K rises to between −160 and −190 μV/K in Figure 3d. The Ag in the $Ag_yPb_{0.99}La_{0.01}Te$ system plays an important role as an effective electron acceptor in reducing the electron carriers and enhancing the thermopower.

Corresponding temperature dependent power factor (σS^2) plots for $Pb_{1-x}La_xTe$ ($x = 0$, 0.01, 0.03, 0.05) and $Ag_yPb_{0.99}La_{0.01}Te$ ($y = 0$, 0.01, 0.03, 0.05, 0.10, 0.15) samples are shown in panels a and b in Figure 4, respectively. For $Pb_{1-x}La_xTe$ samples (Figure 4a), the power factor of $x = 0.03$ and 0.05 increases almost linearly with increasing temperature, but it is relatively small in magnitude; namely for $x = 0.03$, the power factor is ~4 μW/(cm K^2) at ~300 K and ~12 μW/(cm K^2) at ~670 K; for $x = 0.05$, the power factor is ~2 μW/(cm K^2) at ~300 K and ~10 μW/(cm K^2) at ~670 K. Interestingly, for $x = 0.01$, the power factor is weakly temperature dependent and maintains a value between 19 and 22 μW/(cm K^2).

For $Ag_yPb_{0.99}La_{0.01}Te$ samples (Figure 4b), the power factor of $y = 0.01$ increases with temperature from ~12 μW/(cm K^2) at ~300 K to ~21 μW/(cm K^2) at ~720 K. Maximum power factors of ~29 μW/(cm K^2) at ~320 K and ~26 μW/(cm K^2) at ~ 420 K are observed for $y = 0.03$ and 0.05,

(23) Allgaier, R. S.; Scanlon, W. W. *Phys. Rev.* **1958**, *111*, 1029.

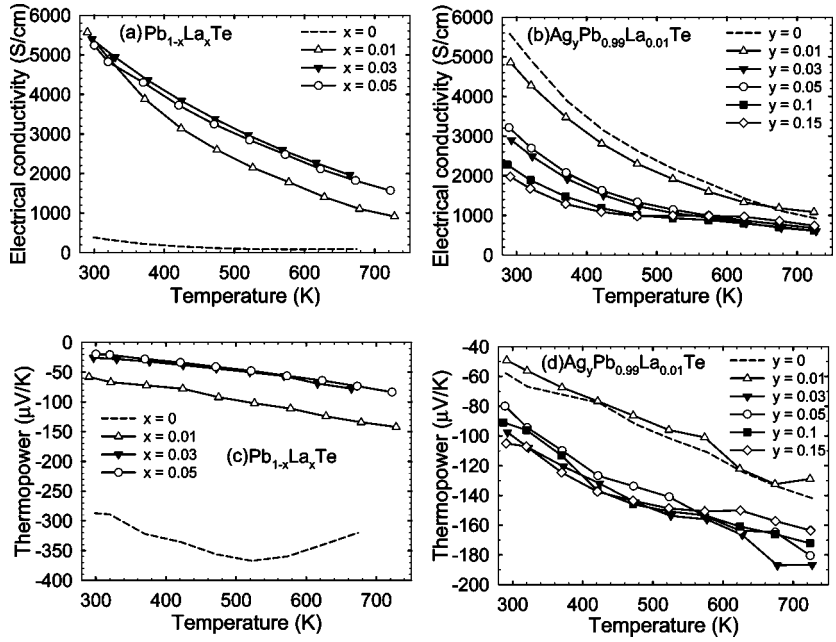

Figure 3. (a) Temperature dependence of electrical conductivity of samples of $Pb_{1-x}La_xTe$ ($x = 0$, 0.01, 0.03, 0.05) and (b) $Ag_yPb_{0.99}La_{0.01}Te$ ($y = 0$, 0.01, 0.03, 0.05, 0.1, 0.15), (c) temperature dependence of thermopower of samples of $Pb_{1-x}La_xTe$ ($x = 0$, 0.01, 0.03, 0.05), and (d) $Ag_yPb_{0.99}La_{0.01}Te$ ($y = 0$, 0.01, 0.03, 0.05, 0.1, 0.15).

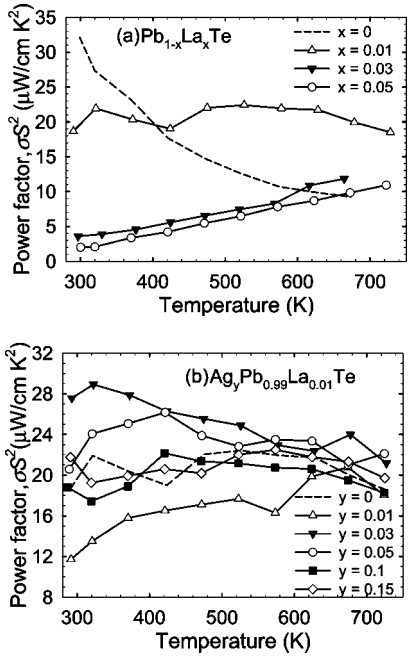

Figure 4. (a) Temperature dependence of power factor of samples of $Pb_{1-x}La_xTe$ ($x = 0$, 0.01, 0.03, 0.05) and (b) $Ag_yPb_{0.99}La_{0.01}Te$ ($y = 0$, 0.01, 0.03, 0.05, 0.1, 0.15).

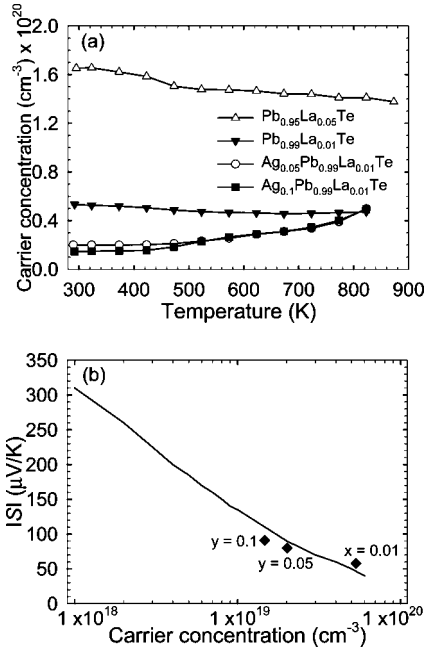

Figure 5. (a) Temperature dependence of carrier concentration of samples of $Pb_{1-x}La_xTe$ ($x = 0.01$) and $Ag_yPb_{0.99}La_{0.01}Te$ ($y = 0.05$, 0.1), and (b) absolute value of the thermopower of various samples as a function of the carrier concentration on a logarithmic scale at room temperature. The solid line is the value calculated from the Pisarenko expression for n-type bulk PbTe with acoustic phonon scattering. The solid diamond symbols indicate each sample ($x = 0.01$ and $y = 0.05$, 0.1).

respectively. These are high power factors and decrease slowly with a further rise in temperature to rather high values of ~22 μW/(cm K^2) at ~720 K. The samples of $y = 0.1$ and 0.15 exhibit power factors between 19 μW/cm K^2 and 22 μW/(cm K^2) over the whole temperature range, which is similar to $Pb_{0.99}La_{0.01}Te$.

The Hall coefficients in the temperature range of 300−820 K were negative indicative of *n*-type conduction, which is consistent with the negative thermopower. Assuming a simple parabolic band and single carrier conduction in our analysis, the carrier concentration n was determined from the relationship $n = 1/eR_H$, where e is the electronic charge and R_H is the Hall coefficient. Figure 5a shows the carrier concentration as a function of temperature for several $Pb_{1-x}La_xTe$ and $Ag_yPb_{0.99}La_{0.01}Te$ samples. For $Pb_{1-x}La_xTe$ samples the carrier concentration was constant with temperature while for $Ag_yPb_{0.99}La_{0.01}Te$ samples we observed a slight increase with increasing temperature. The n value for $Pb_{0.95}La_{0.05}Te$ was ~1.7×10^{20} cm^{-3} at ~300 K, which is about 1 order of magnitude larger than that of $Pb_{0.99}La_{0.01}Te$ (~5.3×10^{19} cm^{-3}); the temperature dependence of the Hall

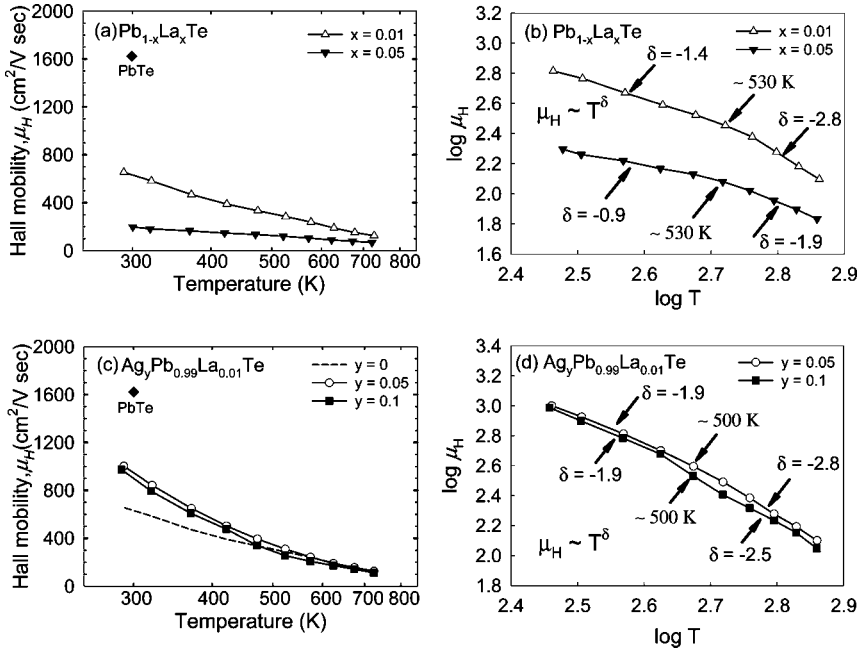

Figure 6. (a) Hall mobility as a function of temperature and (b) log μ_H vs log T plot for samples of $Pb_{1-x}La_xTe$ ($x = 0.01, 0.05$), and (c) Hall mobility as a function of temperature and (d) log μ_H vs log T plot for samples of $Ag_yPb_{0.99}La_{0.01}Te$ ($y = 0, 0.05, 0.1$).

coefficient for $Pb_{0.99}La_{0.01}Te$ was found to be in good agreement with previously reported data.[17]

In $Ag_yPb_{0.99}La_{0.01}Te$, the measured carrier concentration decreased from $\sim 2.0 \times 10^{19}$ cm^{-3} at $\sim$300 K for $y = 0.05$ to $\sim 1.5 \times 10^{19}$ cm^{-3} for $y = 0.1$. In bulk PbTe, in which acoustic phonon scattering dominates, the absolute thermopower values $|S|(n)$ at 300 K can be estimated using the Pisarenko expression:[24,25] $S(\mu V/K) = -477 + 175 \times \log_{10}(n/(1 \times 10^{17}\ cm^{-3}))$. Figure 5b shows the absolute value of thermopower at 300 K as a function of carrier concentration on a logarithmic scale for $Pb_{0.99}La_{0.01}Te$, $Ag_{0.05}Pb_{0.99}La_{0.01}Te$, and $Ag_{0.1}Pb_{0.99}La_{0.01}Te$ (solid diamond symbol). The Pisarenko plot is shown as the full line and it is clear that our samples fall very near this line indicating acoustic phonon scattering. This type of scattering was also reported for $Pb_{1-x}RE_xSe$ (RE = Ce, Pr, Nd, Eu, Gd, and Yb) alloys.[26] The carrier concentration of pure PbTe (S of approximately -290 μV/K at 300 K) used in this work was estimated to be 1×10^{18} to 2×10^{18} cm^{-3} by the Pisarenko expression.

The Hall mobility μ_H was derived from the equation $\mu_H = \sigma/ne$, and the plots with temperature are shown in panels a and b in Figure 6 on a logarithmic scale. The pure PbTe control sample showed the largest Hall mobility of $\sim$1600 cm^2/(V s) at 300 K compared to μ_H of $\sim$650 cm^2/(V s) at 300 K for $Pb_{0.99}La_{0.01}Te$ and $\sim$200 cm^2/(V s) at 300 K for $Pb_{0.95}La_{0.05}Te$. This is in agreement with carrier-concentration dependent mobility at a finite temperature for n-type PbTe samples; for example, $\mu \approx n^{-1/3}$ at 77 K and $\mu \approx n^{-4/3}$ at 4.2 K.[27] In Figure 6b, the power law dependences of $\mu_H \approx T^{-1.4}$ at 290−530 K and $\mu_H \approx T^{-2.8}$ at 530−750 K were observed in $Pb_{0.99}La_{0.01}Te$. $Pb_{0.95}La_{0.05}Te$ has a slower temperature variation $\mu_H \approx T^{-0.9}$ at 300−530 K and $\mu_H \approx T^{-1.9}$ at 530−750 K. The scattering of electron carriers by impurity ions (ionized impurity scattering) may have an influence on the slope change of log μ_H/log T in Figure 6b at $\sim$500 K for $Pb_{1-x}La_xTe$ samples.[28]

The temperature dependence of the mobility is governed by the intensity of thermal vibrations and an energy-dependent mean free path l, thus formulating $l = \Phi(T)\varphi(E)$ where $\varphi(E) \approx E^r$ (r depends on the carrier scattering mechanism and $E \approx T$ for a nondegenerate semiconductor, but the energy of electron is independent of temperature for degenerate semiconductor).[29] The function $\Phi(T)$ is inversely proportional to the number of thermal phonons ($\Phi(T) \approx T^{-s}$, $s = 1, 2$, where s is the number of typical wavelength phonon the electron can collide; for instance, the electron can interact with only one wavelength phonon in the case of $s = 1$), the dependence of mean free path on the temperature and energy is $l \approx E^r T^{-s}$, and thus the mobility becomes $\mu = el/(m\upsilon) \approx T^{-s}E^{r-1/2}$, where e is electron charge, m is electron mass, and υ is electron velocity.[29] It was reported that in a n-type strongly degenerate PbTe sample the mobility followed $\mu \approx T^{-1}$ at 100−300 K and $\mu \approx T^{-2}$ at 300−700 K thus suggesting $\Phi(T) \approx T^{-1}$ (one-phonon process or single-wavelength phonon collision) at low temperature and $\Phi(T) \approx T^{-2}$ (two-phonon process or double-wavelength phonon collision) at high temperature, whereas in a weakly or intermediately degenerate sample the mobility showed $\mu \approx T^{-1.8}$ or $T^{-3/2}$ at 100−200 K and $\mu \approx T^{-5/2}$ at 200−700 K, consequently indicating energy-independent mean free path ($r = 0$).[29,30]

(24) Heremans, J. P.; Thrush, C. M.; Morelli, D. T. *J. Appl. Phys.* **2005**, *98*, 063703.
(25) Thiagarajan, S. J.; Jovovic, V.; Heremans, J. P. *Phys. Status Solidi* **2007**, *1*, 256.
(26) Jovovic, V.; Thiagarajan, S. J.; West, J.; Heremans, J. P.; Story, T.; Golacki, Z.; Paszkowicz, W.; Osinniy, V. *J. Appl. Phys.* **2007**, *102*, 043707.
(27) Kanai, Y.; Nii, R.; Watanabe, N. *J. Appl. Phys.* **1961**, *32*, 2146.
(28) Stavitskaya, T.; Stil bans, L. S. *Fiz. Tverd. Tela* **1960**, *2*, 2082; *Sov. Phys.−Solid State* **1960**, *2*, 1868.
(29) Joffe, A. F.; Stil'bans, L. S. *Rep. Prog. Phys.* **1959**, *22*, 167.
(30) Vinogradova, M. N.; Golikova, O. A.; Efimova, B. A.; Kutasov, V. A.; Stavitskaya, T. S.; Stil'bans, L. S.; Sysoeva, L. M. *Fiz. Tverd. Tela* **1959**, *1*, 1333; *Sov. Phys.−Solid State* **1960**, *2*, 1224.

In this work, the power exponents of ~0.9 at 300−530 K and ~1.9 at 530−750 K for $Pb_{0.95}La_{0.05}Te$ were observed, which is in good agreement with those of 1 at 100−300 K and 2 at 300−700 K for n-type strongly degenerate PbTe samples. It is interesting that the slope change temperature of ~ 530 K in log μ_H/log T for $Pb_{0.95}La_{0.05}Te$ is higher than ~300 K for n-type strongly degenerate PbTe samples (Figure 6b). Thus, the low value of the power exponent at 300−530 K for $Pb_{0.95}La_{0.05}Te$ can be explained in terms of the expected temperature dependent mobility of n-type strongly degenerate PbTe samples.

For the $Pb_{0.99}La_{0.01}Te$ sample, the power exponents are ~1.4 at 290−530 K and ~2.8 at 530−750 K, which are consistent with those of 1.5 at 100−200 K and 2.5 at 200−700 K for n-type intermediately degenerate PbTe samples.[29] Furthermore, the $Pb_{0.99}La_{0.01}Te$ sample nearly follows the Pisarenko expression in terms of acoustic phonon scattering and thus it is not likely that additional competing scattering mechanisms such as ionized impurity scattering play a major role. The thermoelectric properties of strongly doped n-type PbTe in the temperature range of 100−1000 K have been explained completely by the assumption of one type of carrier and the existence of acoustic phonon scattering.[31]

The $Ag_yPb_{0.99}La_{0.01}Te$ samples exhibit a higher room temperature Hall mobility of ~1000 $cm^2/(V\ s)$ for $y = 0.05$ and ~970 $cm^2/(V\ s)$ for $y = 0.1$ compared to ~650 $cm^2/(V\ s)$ of $Pb_{0.99}La_{0.01}Te$ and they also follow the Pisarenko expression, which indicates acoustic phonon scattering. In Figure 6d the power law exponents at 290−500 K for both $Ag_{0.05}Pb_{0.99}La_{0.01}Te$ and $Ag_{0.1}Pb_{0.99}La_{0.01}Te$ are the same as ~1.9 and the respective exponents at 500−750 K are ~2.8 and ~2.5 and thus ionized impurity scattering is negligible. It is interesting that in our samples presented here, the temperature of ~500 K at which the mobility curve deviates from a straight line is much higher than ~300 K and ~200 K reported in n-type strongly degenerate and weakly/intermediately degenerate PbTe samples, respectively.[29]

Thermal Conductivity and Figure of Merit. Panels a and b in Figure 7 show the temperature dependence of the total thermal conductivity κ of $Pb_{1-x}La_xTe$ ($x = 0, 0.01, 0.03, 0.05$) and $Ag_yPb_{0.99}La_{0.01}Te$ ($y = 0, 0.01, 0.03, 0.05, 0.10, 0.15$) samples, respectively. The total thermal conductivity for $x = 0.05$ is ~2.8 W/(m K) at ~720 K, whereas the $x = 0.01$ sample at ~720 K shows ~1.7 W/(m K). The room-temperature total thermal conductivity decreases with increasing y (Ag content) until $y = 0.05$; ~4.7 W/(m K) for $y = 0$, ~4.5 W/(m K) for $y = 0.01$, ~3.1 W/(m K) for $y = 0.03$, and ~2.9 W/(m K) for $y = 0.05$. Beyond $y \approx 0.05$ the room temperature total thermal conductivity increases with increasing y (≈3.2 W/(m K) for $y = 0.1$ and ~3.6 W/(m K) for $y = 0.15$). A total thermal conductivity of ~1.3 W/(m K) at ~ 720 K was observed for $y = 0.03$ and 0.05, which is a ~ 24% reduction compared to ~1.7 W/(m K) for $y = 0$. These values are comparable to those of typical PbTe samples and significantly higher than those of nanostructured PbTe-based samples.[9−11,32]

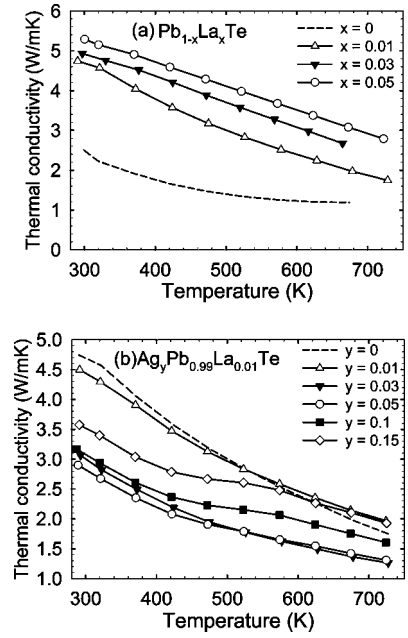

Figure 7. (a) Temperature dependence of the total thermal conductivity of samples of $Pb_{1-x}La_xTe$ ($x = 0, 0.01, 0.03, 0.05$) and (b) $Ag_yPb_{0.99}La_{0.01}Te$ ($y = 0, 0.01, 0.03, 0.05, 0.1, 0.15$).

Generally, the total thermal conductivity has two contributions; the lattice part κ_{latt} and the electronic part κ_{elec}. The κ_{elec} is simply estimated through the Wiedemann−Franz law, which states that $\kappa_{elec} = \sigma TL$ (Lorenz number $L = 1.96 \times 10^{-8}$ $W\Omega/K^2$).[33] Thus, the lattice thermal conductivity κ_{latt} is derived by subtracting the electronic thermal conductivity κ_{elec} from the total thermal conductivity κ. The lattice thermal conductivity κ_{latt} as a function of temperature is shown in panels a and b in Figure 8. The $Pb_{1-x}La_xTe$ samples ($x = 0.01, 0.03, 0.05$) show lower lattice thermal conductivity than pure PbTe ($x = 0$). For $Ag_yPb_{0.99}La_{0.01}Te$ samples, the lattice thermal conductivity decreases with increasing Ag content until $y = 0.05$, but then increases with $y > 0.05$.

The figures of merit (ZT) calculated from the above data for $Pb_{1-x}La_xTe$ and $Ag_yPb_{0.99}La_{0.01}Te$ samples are shown in panels a and b in Figure 9. At 300 K, the $Pb_{1-x}La_xTe$ ($x = 0.01, 0.03, 0.05$) shows ZT values below that of optimized PbTe[5,34] ($ZT \approx 0.4$) and the ZT of ~0.3 and ~0.2 at ~670 K was reached for $x = 0.03$ and 0.05, respectively (ZT of ~0.8 at ~670 K for optimized PbTe). Interestingly, the ZT at ~670 K is ~0.7 for $Pb_{0.99}La_{0.01}Te$, which is comparable to that of optimized PbTe. This is due to the large power factor of ~20 $\mu W/(cm\ K^2)$ at ~670 K. For $Ag_yPb_{0.99}La_{0.01}Te$ samples (Figure 9b), with $y = 0.01$, 0.1, and 0.15, we observed nearly the same figure of merit as for $Pb_{0.99}La_{0.01}Te$. The most impressive enhancement of ZT was observed for

(31) Stavitskaya, T. S.; Long, V. A.; Efimova, B. A. *Fiz. Tverd. Tela* **1965**, *7*, 2554; *Sov. Phys.−Solid State* **1966**, *7*, 2062.

(32) Sootsman, J. R.; Pcionek, R. J.; Kong, H.; Uher, C.; Kanatzidis, M. G. *Chem. Mater.* **2006**, *18*, 4993.

(33) Kumar, G. S.; Prasad, G.; Pohl, R. O. *J. Mater. Sci.* **1993**, *28*, 4261.

(34) Gelbstein, Y.; Dashevsky, Z.; Dariel, M. P. *Phys. B* **2005**, *363*, 196.

(35) Hunter, B. A. Rietica−A visual Rietveld program. International Union of Crystallography Commission on Powder Diffraction Newsletter; International Union of Crystallography Commission on Powder Diffraction: Chester, U.K., summer 1998;No. 20, available at http://www.rietica.org.

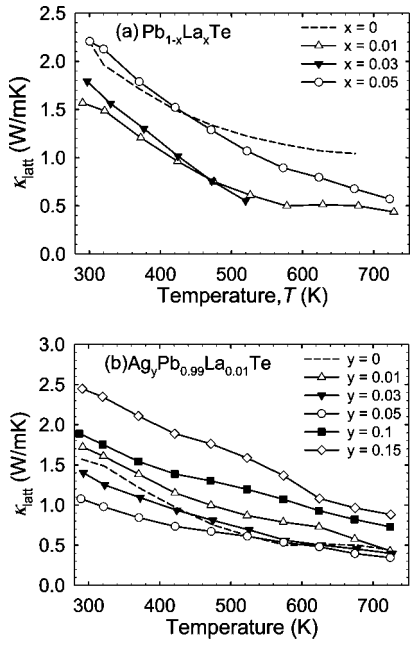

Figure 8. (a) Temperature dependence of the lattice thermal conductivity of samples of $Pb_{1-x}La_xTe$ ($x = 0$, 0.01, 0.03, 0.05) and (b) $Ag_yPb_{0.99}La_{0.01}Te$ ($y = 0$, 0.01, 0.03, 0.05, 0.1, 0.15).

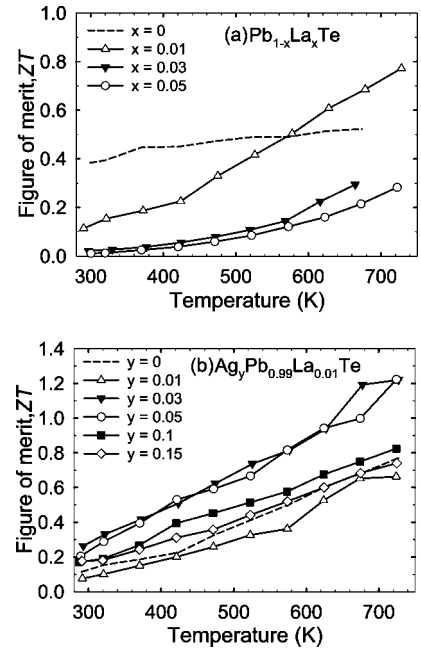

Figure 9. (a) Temperature dependence of the thermoelectric figure of merit of samples of $Pb_{1-x}La_xTe$ ($x = 0$, 0.01, 0.03, 0.05) and (b) $Ag_yPb_{0.99}La_{0.01}Te$ ($y = 0$, 0.01, 0.03, 0.05, 0.1, 0.15).

the samples with $y = 0.03$ and 0.05. The *ZT* of these samples surpassed that of $Pb_{0.99}La_{0.01}Te$ over the entire temperature range and reached the highest value of ~1.2 at ~720 K, which is a significant improvement compared to the *ZT* of ~0.8 at ~ 720 K for optimized PbTe. This large improvement is attributed mainly to the high power factor of ~22 μW/(cm K^2) at ~720 K.

Concluding Remarks. The low level substitution of La (≤5 at.%) for Pb in PbTe introduces effective electron donors in the lattice and considerably enhances the electrical conductivity. The Ag acts as an electron acceptor in $Ag_yPb_{0.99}La_{0.01}Te$ and allows one to counteract the donor property of La. The 5 mol % Ag doping in $Pb_{0.99}La_{0.01}Te$ diminishes the electron carrier concentration by approximately a factor of 2 in comparison to $Pb_{0.99}La_{0.01}Te$. The mobility of these heavily doped samples remains remarkably high even at high temperature and its temperature dependence is similar to those of n-type strongly degenerate or intermediately degenerate PbTe samples. The $Ag_yPb_{0.99}La_{0.01}Te$ samples show high power factors of >18 μW/(cm K^2) at ~720 K. A maximum *ZT* of ~1.2 at ~720 K was achieved for the composition $Ag_{0.05}Pb_{0.99}La_{0.01}Te$, which shows a power factor of ~22 μW/(cm K^2) at ~720 K.

Acknowledgment. This work was supported by the Office of Naval Research.

CM803437X